

RESEARCH ARTICLE

10.1002/2014JC010397

On the origin and propagation of Denmark Strait overflow water anomalies in the Irminger Basin

Kerstin Jochumsen¹, Manuela Köllner^{1,2}, Detlef Quadfasel¹, Stephen Dye^{3,4}, Bert Rudels⁵, and Heðinn Valdimarsson⁶

Key Points:

- Temperature anomalies propagate from Denmark Strait to Angmagssalik
- Entrainment modifies salinity within the first 180 km downstream of the sill
- Changes in the mixing ratio are important for the downstream variability

Supporting Information:

- Figures S1 and S2

Correspondence to:

K. Jochumsen,
kerstin.jochumsen@uni-hamburg.de

Citation:

Jochumsen, K., M. Köllner, D. Quadfasel, S. Dye, B. Rudels, and H. Valdimarsson (2015), On the origin and propagation of Denmark Strait overflow water anomalies in the Irminger Basin, *J. Geophys. Res. Oceans*, 120, 1841–1855, doi:10.1002/2014JC010397.

Received 21 AUG 2014

Accepted 4 FEB 2015

Accepted article online 12 FEB 2015

Published online 19 MAR 2015

¹Institut für Meereskunde (CEN), Universität Hamburg, Hamburg, Germany, ²Now at Helmholtz Centre for Ocean Research (GEOMAR), Kiel, Germany, ³Centre for Environment, Fisheries and Aquaculture Science, Lowestoft, UK, ⁴Centre for Ocean and Atmospheric Sciences, School of Environmental Sciences, University of East Anglia, Norwich, UK, ⁵Finnish Meteorological Institute, Helsinki, Finland, ⁶Marine Research Institute, Reykjavik, Iceland

Abstract Denmark Strait Overflow Water (DSOW) supplies the densest contribution to North Atlantic Deep Water and is monitored at several locations in the subpolar North Atlantic. Hydrographic (temperature and salinity) and velocity time series from three multiple-mooring arrays at the Denmark Strait sill, at 180 km downstream (south of Dohrn Bank) and at a further 320 km downstream on the east Greenland continental slope near Tasiilaq (formerly Angmagssalik), were analyzed to quantify the variability and track anomalies in DSOW in the period 2007–2012. No long-term trends were detected in the time series, while variability on time scales from interannual to weekly was present at all moorings. The hydrographic time series from different moorings within each mooring array showed coherent signals, while the velocity fluctuations were only weakly correlated. Lagged correlations of anomalies between the arrays revealed a propagation from the sill of Denmark Strait to the Angmagssalik array in potential temperature with an average propagation time of 13 days, while the correlations in salinity were low. Entrainment of warm and saline Atlantic Water and fresher water from the East Greenland Current (via the East Greenland Spill Jet) can explain the whole range of hydrographic changes in the DSOW measured downstream of the sill. Changes in the entrained water masses and in the mixing ratio can thus strongly influence the salinity variability of DSOW. Fresh anomalies found in downstream measurements of DSOW within the Deep Western Boundary Current can therefore not be attributed to Arctic climate variability in a straightforward way.

1. Introduction

The passage featuring the largest transport of dense water from the Nordic Seas into the North Atlantic is Denmark Strait, one of the few deep channels in the Greenland-Scotland-Ridge (GSR). The dense water, known as Denmark Strait Overflow Water (DSOW), provides about half of the total dense water overflow of the GSR, thus contributing significantly to the formation of lower North Atlantic Deep Water [Hansen *et al.*, 2004]. The overflow is steered by topography and descends as a gravity plume along the East Greenland shelf break and continental slope into the Irminger Basin [Dickson and Brown, 1994; Dickson *et al.*, 2002]. DSOW in the northern Irminger Basin is commonly defined as a water mass with a potential density anomaly of more than 27.8 kg m^{-3} and being colder than 2°C [e.g., Tanhua *et al.*, 2005] with a salinity of about 34.9. Along its way, mixing with ambient waters modifies the temperature, salinity, and other characteristics of the overflow plume and its volume transport is substantially increased. The DSOW then spreads into the abyssal subpolar North Atlantic as the bottom layer of the Deep Western Boundary Current (DWBC), which is monitored with moored instruments at several locations [Fischer *et al.*, 2014].

Downstream of Denmark Strait, entrainment warms the overflow and hence decreases its density. Nevertheless, DSOW remains the densest water mass in the Irminger Sea with temperatures below 2°C , descending to more than 2000 m depth. Here it is overlain by Iceland Scotland Overflow Water (ISOW), which also influences the less dense portion of the plume by isopycnal mixing. The average overflow water transport at the sill of Denmark Strait is around 3.4 Sv [Jochumsen *et al.*, 2012], which increases further downstream to 10.7 Sv near Angmagssalik due to entrainment and the combination with ISOW [Dickson *et al.*, 2008].

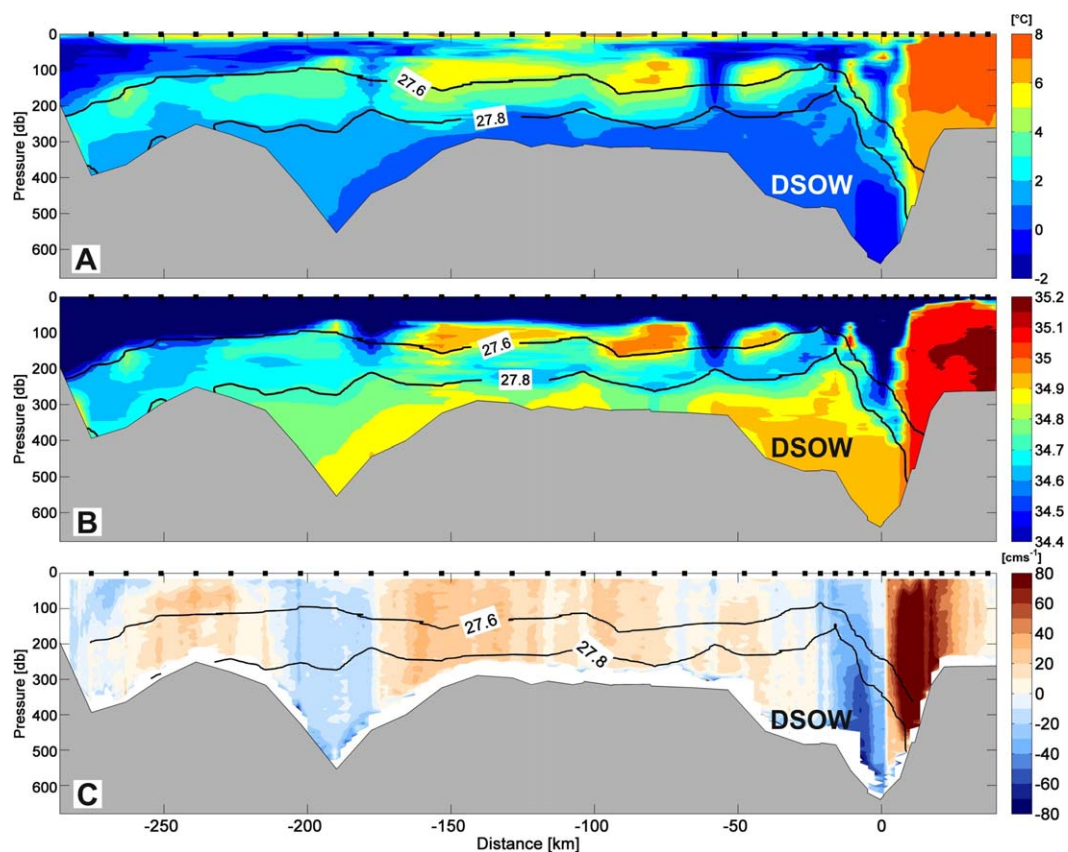


Figure 1. Snapshots of the (a) potential temperature, (b) salinity, and (c) velocity distribution at the sill of Denmark Strait in July/August 2012 as measured during Poseidon cruise P437-1. The low salinity of the surface water is out of scale; thus, the upper layer was filled with dark purple color. The velocity was obtained from a vessel-mounted ADCP with 75 kHz frequency. No data are available at shallow and near-bottom depth levels due to interference with surface/bottom reflection. The data were detided using a tidal model and rotated according to the direction of the section; shown is the cross-section component. Negative velocities are toward the southwest (blue), while positive velocities are northeastward (red). Black lines illustrate selected isopycnals. The Denmark Strait overflow water with $\sigma_\theta > 27.8 \text{ kg m}^{-3}$ is labeled as DSOW; note the extension of this layer toward Greenland. The positions of CTD stations are marked at the top of each figure. The ADCP data have a spatial resolution of about 3 km. The location of the section is shown in Figure 2.

DSOW measurements in Denmark Strait focused on the deep channel where the velocity is strong ($>0.5 \text{ m s}^{-1}$ on average), although it has long been known that a distinct layer of dense water in the DSOW density range also is present on the Greenland shelf (Figure 1). The relevance of this layer is assumed to be small, as the synoptic current velocity sections obtained during ship cruises were small ($<0.1 \text{ m s}^{-1}$ on average, when considering also the recirculations; Figure 1c) [Macrandar *et al.*, 2007; Jochumsen *et al.*, 2012]. At the sill of Denmark Strait, the DSOW layer thickness varies between 50 and 300 m [Macrandar *et al.*, 2007]. Plume thickness variability is large along the descending pathway due to the presence of eddies containing various overflow thicknesses [Käse *et al.*, 2003]. The downstream overflow layer is often covered by a low-salinity lid [e.g., Rudels *et al.*, 1999] and its upper part is stratified in temperature [Dickson *et al.*, 2008], but the lower 100 m of the plume are cold and almost homogeneous. At the Angmagssalik mooring array, approximately 500 km downstream of the sill, DSOW is found at depths greater than 1400 m. Here the average layer thickness (for $\sigma_\theta > 27.8 \text{ kg m}^{-3}$) is 300–600 m with variations of $\pm 150 \text{ m}$. The layer thickness depends on the location of the measurement on the Greenlandic slope [Dickson *et al.*, 2008, 1999], as the layer thickness increases with depth and thus with distance from Greenland and also incorporates some of the ISOW of similar density.

Denmark Strait is wider than the baroclinic Rossby radius, which is 14 km at these latitudes [Whitehead, 1998]. Thus, mesoscale eddies can be present in the DSOW plume at the sill and along the descending pathway of the overflow, generated by vortex stretching [Spall and Price, 1998] and/or baroclinic instability [Swaters, 1991]. In Eulerian measurements, these eddies are seen as DSOW plume pulses in the velocity

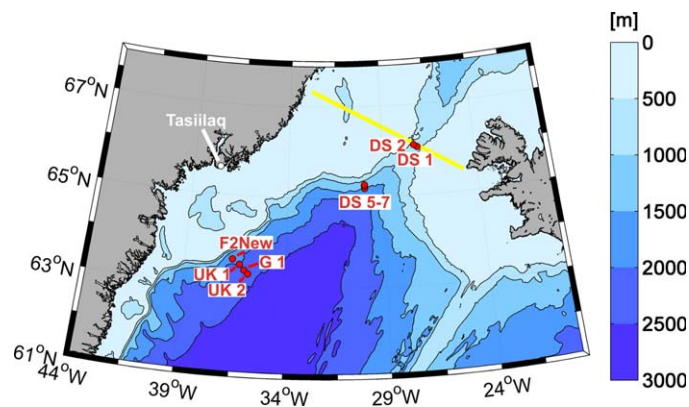


Figure 2. Map of the mooring positions. The three arrays addressed in this work are located (1) at the sill of Denmark Strait (Denmark Strait sill array: DS 1 and DS 2), (2) 180 km downstream at 30°W (entrainment array: DS 5, DS 6, and DS 7), and (3) 550 km downstream off Tasiilaq, formerly Angmagssalik (Angmagssalik array: F2New, UK 1, G 1, and UK 2). The location of the section shown in Figure 1 is marked by the yellow line.

time series at high frequencies and are often correlated with the lowest temperatures. The periods associated with them are 2–10 days at the sill of Denmark Strait, but a shift to longer time scales occurs downstream [Voet and Quadfasel, 2010], with dominating periods close to 10 days near Angmagssalik [Fischer et al., 2014]. Observations from mooring arrays downstream of Denmark Strait revealed the dominance of horizontal stirring by these mesoscale eddies for the entrainment of ambient water into the overflow plume

[Voet and Quadfasel, 2010], while vertical mixing through shear instabilities was found to dominate the entrainment only within 100 km distance from Denmark Strait sill [Paka et al., 2010]. This hypothesis was supported by microstructure measurements by Paka et al. [2013], who concluded that vertical turbulent mixing is not the major process controlling entrainment in the DSOW plume at ~200 km from the sill. Detailed process studies on the entrainment in the region close to the sill of Denmark Strait are lacking; it is therefore still unclear which process dominates the entrainment in this specific region. Further downstream, the overflow, now the deepest layer of the DWBC, still exhibits variability on various time scales, e.g., from multidecadal to weekly close to Cape Farewell [van Aken and de Jong, 2012], where the strongest changes occur at the longest of these time scales.

In this work, we use hydrographic and velocity measurements from three mooring arrays along the DSOW pathway to deduce the relative role of advection of varying source waters versus mixing for the changing plume characteristics in the Irminger Sea. We focus our study on the nearly homogeneous bottom part of the DSOW plume, as most data were collected by near-bottom instruments. Our aim is to understand the changes of the physical properties of the DSOW plume on its descent into the deep Irminger Basin, as it joins the DWBC. By correlating observations from the sill of Denmark Strait with downstream measurements, we will follow the propagation pathway of anomalies. Thereby we obtain advection time scales of anomalies as well as the average entrainment rates of ambient water. The variability of the DSOW properties is discussed and related to variability in the mixing ratio. Our work highlights the influence of entrainment on downstream DSOW properties: the origins of anomalies in temperature and salinity have to be considered when interpreting DSOW anomalies in the subpolar North Atlantic.

2. Instruments, Data Quality Control, Processing, and Dependencies

2.1. Setup of Mooring Arrays

The analysis presented here is based on near-bottom records of moored instruments from three different mooring arrays, obtained in the period 2007–2012 (Figure 2). All arrays were designed to monitor the Denmark Strait Overflow Water as it enters the North Atlantic Ocean and descends from the sill of Denmark Strait (~630 m maximum depth) to the bottom of the Irminger Basin (~3000 m depth near Cape Farewell). The northernmost array was placed directly at the sill of Denmark Strait (DS 1 and DS 2; we refer to it as the Denmark Strait sill array). Three moorings were operated downstream of the sill (DS 5, DS 6, and DS 7), which in the following are referred to as the entrainment array; and four moorings were located south of Tasiilaq (the name of the settlement on the coast of Greenland was changed from Angmagssalik to Ammassalik (modern Danish spelling) and later to Tasiilaq (Greenlandic), we use the name Angmagssalik here for the mooring array to stay consistent with older literature) (F2New, UK 1, G 1, and UK 2; referred to as the Angmagssalik array). The two moorings DS 1 and DS 2 were at 630 and 570 m depth and the distance between the two moorings was 10 km. The moorings at the entrainment array were placed at 1460, 1360,

and 1270 m depth and separated by a distance of 4.5 km. The Angmagssalik array covered the continental slope with F2New at 1770 m, UK 1 at 1970 m, G 1 at 2150 m, and UK 2 at 2350 m depth (distance between moorings: 10–25 km). The locations of the moorings are depicted in Figure 2. Single deployments lasted 1 or 2 years and the temporal resolution of all measurements is 10 or 20 min. The entrainment array was only deployed once and the data cover ~ 1 year. The moorings were equipped with either Aanderaa current meters (RCM 8, RCM 11, or Seaguard) or with Workhorse ADCPs (75 or 150 kHz; range ~ 600 and 350 m; bin size 16 or 8 m), as well as SeaBird SBE37SM MicroCATs (MCs).

Since 2007, the mooring work at the sill of Denmark Strait (the mooring program at the sill of Denmark Strait was originally a cooperation between the Nordic countries with the funding of the Nordic Council of ministers. It was initiated in 1994–1995, but the observation started in 1996. A German group (IFM Kiel) joined the measuring effort in 1999 under the SFB460 program. First results of a 4 year period were published in *Macrander et al.* [2005, 2007].) is a joint effort of the University of Hamburg (Germany) and the Marine Research Institute (Reykjavik, Iceland) in the framework of the European THOR (Thermohaline Overturning at Risk?, 2008–2012, which also funded the entrainment array) and NAACLIM (North Atlantic Climate, ongoing since 2012) projects and national German funding. The most recent results from the measured ADCP velocity time series are presented in *Jochumsen et al.* [2012] and *Fischer et al.* [2014].

Recent mooring deployments at the cooperative Angmagssalik array (the Angmagssalik array was set up in 1986 by the UK's Ministry of Agriculture Food and Fisheries (Lowestoft Laboratory—now named Cefas) on the east Greenland continental slope at about 63°N. From 1995, it was maintained by collaboration by UK (Cefas), German (University of Hamburg), and Finnish teams as part of multiple national programs and the EU-funded projects VEINS (Variability of Exchanges in the Northern Seas, 1997–2000), ASOF (Arctic Sub-Arctic Ocean Flux, 2003–2005), and THOR) were carried out primarily by Cefas and consisted of four current meter moorings also equipped with MCs. The moorings were deployed at the continental slope to cover the dense overflow water from the Denmark Strait. A number of studies on mixing, transport, and water mass variability using the Angmagssalik array data have been published over the last 20 years in, e.g., *Dickson and Brown* [1994], *Dickson et al.* [2008], *Voet and Quadfasel* [2010], and *Hall et al.* [2011].

Instruments in all arrays were deployed close to the bottom; the records used in this work were obtained from measurements at least 15 m above the seafloor.

2.2. Measurement Accuracies

The accuracy of the current speed measurement is $\pm 1 \text{ cm s}^{-1}$ for the RCM 8 instruments and $\pm 0.15 \text{ cm s}^{-1}$ for RCM 11 acoustic current meters, with $\pm 5^\circ$ for the direction. Hourly ADCP ensembles were obtained with a velocity standard deviation of $\pm 0.8 \text{ cm s}^{-1}$, but averaged in the postprocessing to further reduce errors [cf. *Jochumsen et al.*, 2012]. To compare data from the different arrays and instruments, we focus on velocity time series obtained at discrete depth levels. For the Denmark Strait sill array, we use the velocity from the bin of maximum downstream flow as measured by the ADCPs (found 120 m above the bottom at DS 1 and 80 m above the bottom at DS 2) to avoid effects of bottom friction and ringing (which is a known instrument error for the deepest bins). At Angmagssalik, the deepest current meter record from each mooring is analyzed (depth above bottom 15–20 m). Current velocities at Angmagssalik are lower than at Denmark Strait and consequently also the frictional boundary layer is thinner. Unfortunately, ADCP velocities from the entrainment array could not be used due to large tilts of the instruments from mooring knock-down during most of the deployment period. All velocity vectors were rotated in the direction of the average flow and only the downstream component is considered here. The overall error of the velocity time series used in this study is below 5%.

The accuracy of the factory calibrated MicroCAT measurements is $\pm 0.002^\circ\text{C}$ for temperature and ± 0.0015 for salinity. The MC measurements were generally tested against CTD measurements with a calibration cast before or after deployment. The differences between the two instruments (MC and CTD) at the calibration casts were $< 0.005^\circ\text{C}$ for temperature and < 0.005 for salinity for working devices. Nevertheless, some salinity time series obtained by the MCs showed sudden shifts within a record or unrealistic drift, which could not be corrected. These data were removed and excluded from the analysis presented here (salinity at DS 1 in 2007–2008, at G 1 in 2009–2010, and at UK 1 in 2007–2009). The periods of remaining, quality-controlled data are presented in Figure 3.

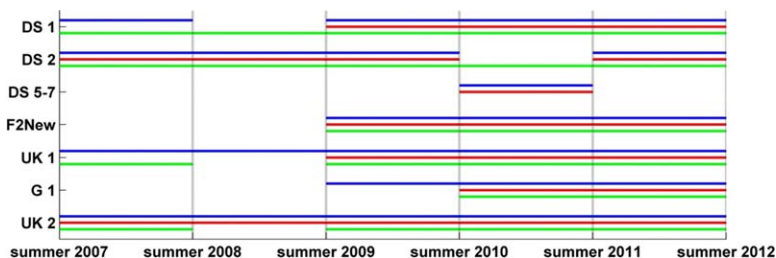


Figure 3. Quality-controlled data availability from 2007 to 2012. Blue: temperature data, red: salinity data, green: velocity data. Moorings were serviced in summer, which refers to the months June, July, and August.

2.3. Processing and Filtering

Further processing was applied to the MC time series: (1) removal of outliers by comparing single data points with the neighboring data points. When differences between a data point and its neighbors exceeded twice the standard deviation of the whole time series, the point was removed. Outliers were only found in salinity data. (2) Applying a density threshold for overflow water. Only anomalies of DSOW were considered in this study; hence, all potential density anomalies $<27.80 \text{ kg m}^{-3}$ were removed. These post-processing steps affected less than 0.2% of the data. Finally, all time series were averaged to 1 day means to remove high-frequency signals. Tidal signals were not present in the temperature and salinity time series and were removed from the velocity data by low-pass filtering (20 day Hamming window, see below).

Eddy activity has been noted previously at the sill of Denmark Strait on time scales of a few days [Girton *et al.*, 2001], as well as eddy generation downstream of Denmark Strait sill [Kåse *et al.*, 2003]. All our hydrographic near-bottom measurements confirmed the persistence of DSOW along the Greenland slope; whether a passing eddy, carrying the “DSOW lenses” described in von Appen *et al.* [2014a], was present or not. When comparing the observations at the sill to those at Angmagssalik, it is seen that the overall high-frequency variance of the overflow plume is much reduced downstream and shifted to longer time scales [Voet and Quadfasel, 2010; Fischer *et al.*, 2014]. Thus, the time scale of the synoptic eddies changed between the mooring arrays. The hydrographic time series between the three mooring arrays show only low correlations at the original daily resolution ($r < 0.25$, calculated with lags between 2 and 20 days). As these correlations explain only 6% and less of the variance, we conclude that single eddies are likely not traceable and probably merge with each other or fade along the descending pathway. In order to compare the time series with each other, synoptic-scale variations must be removed, and here filtered time series representing a mean state over several eddies were used for the analysis. A 20 day low-pass filter was applied (using a Hamming window) to all time series. The window size was chosen in agreement with minima of energy identified in a spectral analysis of the data for all three mooring arrays (not shown) [see Fischer *et al.*, 2014].

While the application of a low-pass filter is a common practice in handling velocity time series for reducing the small-scale variability and removing tides, filtering hydrographic data may act as false mixing. The effect of the filter on the temperature and salinity data was therefore checked carefully for each mooring array. The filtered properties were compared to the original data (including the synoptic-scale variability) using T/S diagrams; the T/S space covered by the data was reduced due to the filter. Changes were small for the Denmark Strait and Angmagssalik arrays. Only at the entrainment array did the filter reduce the range of data notably. For the entrainment array, the filter constrained the data to a T/S space in the center of the original data points. Although no artificial water masses were produced, the smoothing of the variability due to the filter reduced the amplitude of T/S oscillations. The effect of the filter is therefore comparable to artificial mixing at this location. Thus, passing DSOW eddies with pronounced fresh and cold signals were averaged with the background T/S properties due to the filter, resulting in moderate temperature and salinity variations.

2.4. Correlation Coefficients

Correlations were computed for all time series within each separate mooring array to analyze the uniformity of the flow and the relation between their time series. Here we discuss only coefficients above the 99% significance level ($p < 0.01$). Filtering reduces the independence of sequential measurements and this change in the effective degrees of freedom was taken into account for the calculations of p values. Critical

Table 1. Mean Near-Bottom Potential Temperatures (°C), Salinities, Potential Density Anomalies (kg m^{-3}), and Downstream Velocities (cm s^{-1}) With Standard Deviation (of the Filtered Time Series) at All Moorings; n.a.: not available.

	Potential Temperature	Salinity	Potential Density Anomaly	Downstream Velocity
DS 1	-0.08 ± 0.13	34.898 ± 0.003	28.03 ± 0.01	31.1 ± 6.9
DS 2	0.15 ± 0.17	34.899 ± 0.006	28.02 ± 0.01	50.9 ± 9.3
DS 5	1.10 ± 0.21	34.897 ± 0.008	27.96 ± 0.01	n.a.
DS 6	1.07 ± 0.21	34.888 ± 0.009	27.95 ± 0.01	n.a.
DS 7	1.18 ± 0.20	34.898 ± 0.008	27.95 ± 0.01	n.a.
F2New	2.00 ± 0.17	34.894 ± 0.011	27.89 ± 0.01	22.8 ± 2.5
UK 1	1.73 ± 0.16	34.890 ± 0.011	27.90 ± 0.01	23.8 ± 3.2
G 1	1.45 ± 0.15	34.895 ± 0.009	27.93 ± 0.01	24.2 ± 4.6
UK 2	1.27 ± 0.14	34.890 ± 0.010	27.94 ± 0.01	21.8 ± 5.1

correlation coefficients for the filtered time series are dependent on the length of the time series and amount $r=0.56/r=0.35/r=0.27$ for 1/3/5 year records. Significant and nonsignificant correlations are indicated separately in Tables (2–5). The correlations were calculated from anomalies, calculated as deviations from the mean of each individual time series.

Additionally, all physical parameters were correlated between the mooring arrays to identify similarities and to obtain the advection time scales. The time lag was varied from zero to 50 days; the strongest significant correlation was then chosen as the advection time. The lags obtained from the analysis have an uncertainty of a few days due to the filtering process: the resulting correlation coefficients are very similar for a time span of ± 2 days. The longest overlapping period of measurements was always considered. For example, the records of DS 1 and G 1 were correlated for the period 2009–2012, while the single-year data set of 2007–2008 was not taken into account (cf. Figure 3). Naturally, all correlations given for DS 5, DS 6, and DS 7 are based on the 1 year deployment in 2010–2011.

3. Results

3.1. Variability and Correlations Within the Mooring Arrays

The near-bottom measurements from the three mooring arrays were obtained at diverse locations and depth levels. The shallowest mooring of an array generally exhibits higher temperatures and less dense water (Table 1). Within the Denmark Strait sill array, the average temperature at the shallower mooring DS 2 is 0.23°C higher than at DS 1. Similar results are obtained for the two southern mooring arrays: a temperature difference of 0.08°C is apparent between DS 7 and DS 5. An exception is mooring DS 6, where colder water was found when compared to the shallower DS 7 and deeper DS 5 (Figure 4). Nevertheless, there is no significant difference in density between these moorings due to the salinity distribution (Table 1). At Angmagssalik, the average temperature at F2New is 0.73°C higher than at UK 2. Differences in the average salinity within the mooring arrays are small (below ± 0.01) and often close to the accuracy of the measurements (see Figure 5). The average downstream velocity is high at the sill of Denmark Strait ($30\text{--}50 \text{ cm s}^{-1}$)

and lower at Angmagssalik (below 25 cm s^{-1}), where the plume is spread over a larger area.

The variability within one mooring array is often similar for the hydrographic time series, which is seen in the strong correlations obtained for the records within close proximity (Tables 2 and 3). Highest correlations in temperature are found at the entrainment array, between DS 5 and DS 6 ($r = 0.98$), and at Angmagssalik for salinity ($r = 0.96$ for the neighboring moorings F2New and UK 1, UK 1 and G 1, G 1 and UK 2). Correlations

Table 2. Internal Correlations of Moored Near-Bottom Time Series (Low-Pass Filtered) From the Denmark Strait Sill and Entrainment Arrays^a

	Correlation Coefficient r			
	DS 1–DS 2	DS 5–DS 6	DS 6–DS 7	DS 5–DS 7
Potential temperature	0.84	0.98	0.97	0.92
Salinity	0.57	0.86	0.91	0.82
Downstream velocity	0.37	n.a.	n.a.	n.a.

^aAll correlations were calculated with no time lag, as anomalies are expected to occur approximately simultaneously at all moorings within an array (located on a section perpendicular to the mean flow). Current velocities were rotated to the dominant flow direction and only the downstream component was used. At Denmark Strait sill three 1 year periods with overlapping data exist for the hydrographic data, while the entrainment array covered only one deployment period (cf. Figure 3). n.a.: not available.

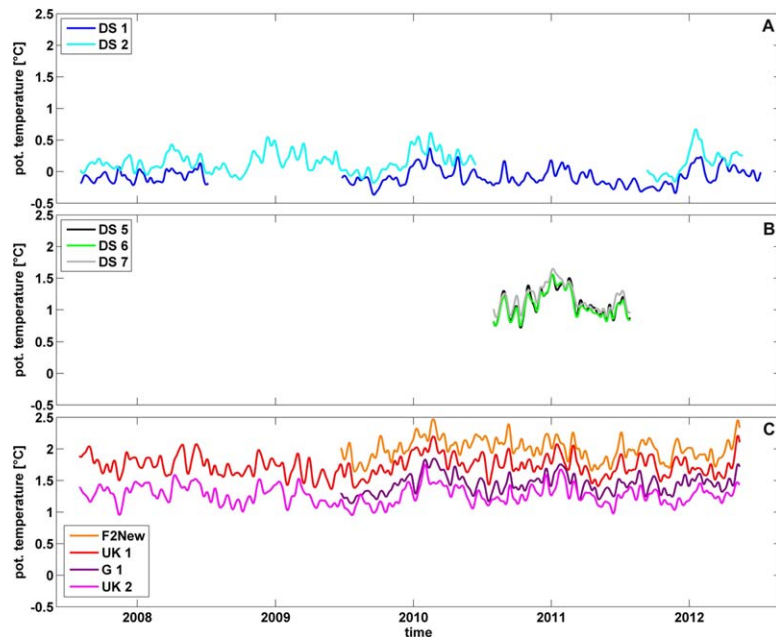


Figure 4. Low-pass filtered bottom potential temperature time series for all three mooring arrays. See Figure 1 for the locations of the arrays. (a) Denmark Strait sill array. (b) entrainment array. (c) Angmagssalik array.

decrease with distance between the moorings, which is most obviously seen in the temperature correlations of F2New with the other moorings at Angmagssalik (Table 3). The only correlation below $r = 0.8$ in salinity is apparent at Denmark Strait sill, where the shallower DS 2 records show a higher variability with pronounced low-salinity events, which are absent at DS 1. The overall variance found in salinity increases downstream (see Figure 5), which is reflected in the elevated standard deviations of the records obtained at Angmagssalik (Table 1). The downstream increase of variance in salinity suggests that the overflow sources in the Nordic Seas are relatively stable in salinity. The downstream variance is elevated by the entrainment of neighboring water masses. In contrast, temperature already exhibits considerable variability at the

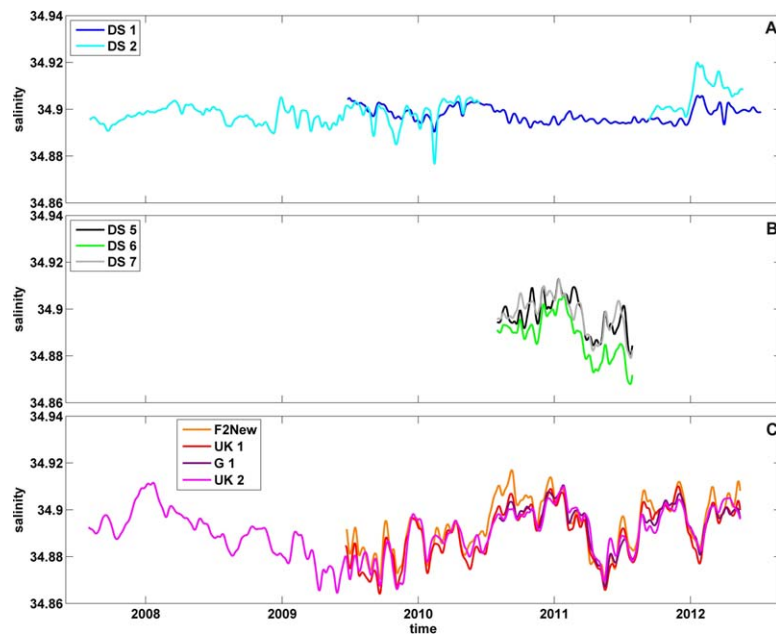


Figure 5. Low-pass filtered bottom salinity time series for all three mooring arrays. See Figure 1 for the locations of the arrays. (a) Denmark Strait sill array. (b) entrainment array. (c) Angmagssalik array.

Table 3. Correlations of Moored Time Series From the Angmagssalik Array (Low-Pass Filtered), Similar to Table 2^a

	Correlation Coefficient <i>r</i>					
	F2New-UK 1	F2New-G 1	F2New-UK 2	UK 1-G 1	UK 1-UK 2	G 1-UK 2
Potential Temperature	0.88	0.55	0.46	0.73	0.61	0.87
Salinity	0.96	0.91	0.87	0.96	0.92	0.96
Downstream velocity	0.29	−0.00	0.11	0.20	− 0.30	0.25

^aNonbolded numbers denote correlations below the 99% significance limit. Bolded numbers correspond to significant correlations.

northernmost moorings at the sill of Denmark Strait and the impact of entrainment on the variance of this property is not as pronounced.

Seasonal variability is on the order of $\pm 0.1^\circ\text{C}$ for temperature at the Denmark Strait sill and Angmagssalik arrays (derived from a harmonic analysis), explaining about 10% of the variance. The records from the entrainment array are too short to derive seasonal information. The seasonal amplitude in salinity is 0.002 at the Denmark Strait sill (below measurement accuracy) and 0.008 at Angmagssalik. The variance induced by the seasonal cycle is thus increasing downstream; only 5% is explained by seasonality at the sill, while 10% can be attributed to the seasons at Angmagssalik. These contributions to the variance were obtained from the low-pass filtered time series; the seasonal effect is even less pronounced for the unfiltered time series [cf. Jochumsen *et al.*, 2012].

In contrast to the hydrographic variability, velocity fluctuations within the separate arrays (time series shown in the supporting information, Figure S1) are only weakly correlated with $r < 0.4$ at all locations (Tables 2 and 3); often no significant correlation was found at all. These low correlations are likely caused by fluctuations in the plume position: the current core migrates between shallower and deeper positions along the Greenland shelf and slope [Dickson *et al.*, 1999]. An indicator for the varying position is the negative correlation between UK 1 and UK 2: at these time scales the current is either strong at UK 1 or at UK 2, not at both positions simultaneously. In a synoptic sense, the current core is about 20–30 km in width at Angmagssalik [cf. Fischer *et al.*, 2014, Figure 5a] and therefore never covers all moorings simultaneously, which are 10–25 km apart from each other. Seasonal variations of the downstream velocities are 3–5 cm s^{-1} at the Denmark Strait sill with maximum velocities in winter. At Angmagssalik, the seasonal amplitude is in the order of 1 cm s^{-1} and not significant, confirming the results from Dickson and Brown [1994].

Correlations between the different parameters (temperature, salinity, and velocity) are weak ($r < 0.4$). Only at the entrainment array, where the moorings are in close proximity, do salinity and temperature fluctuations occur in phase ($r > 0.6$). In general, positive velocity anomalies coincide with negative temperature anomalies, but this anticorrelation is again weak ($-0.1 > r > -0.3$). Thus, the maximum velocities within the overflow plume are not associated with extreme temperatures and salinities. Overflow eddies rather displace isopycnals above the plume and the effect cannot be noticed in our near-bottom measurements.

3.2. Signal Propagation Along the Greenland Continental Slope

Lagged correlations are used to relate anomalies registered at the Denmark Strait sill with downstream signals and to obtain propagation times. The correlation coefficients found for all potential temperature time series are given in Table 4 as well as the time lags used to obtain these correlations. Significant correlations

Table 4. Lagged Correlations of Potential Temperature (Low-Pass Filtered) Between the Three Mooring Arrays^a

	Correlation Coefficient <i>r</i>						
	Potential Temperature						
	DS 5	DS 6	DS 7	F2New	UK 1	G 1	UK 2
DS 1	0.78(2d)	0.77(1d)	0.67(2d)	0.34(11d)	0.41(10d)	0.57(13d)	0.53(16d)
DS 2	n.a.	n.a.	n.a.	0.76(8d)	0.51(13d)	0.75(15d)	0.61(16d)
DS 5	–	–	–	0.39(11d)	0.59(11d)	0.70(12d)	0.71(14d)
DS 6	–	–	–	0.43(10d)	0.64(11d)	0.78(11d)	0.77(14d)
DS 7	–	–	–	0.52(10d)	0.70(10d)	0.80(11d)	0.79(14d)

^a(xxd): days of lag. n.a.: not available. Nonbolded numbers denote correlations below the 99% significance limit. Bolded numbers correspond to significant correlations. Dashes are filled in for the autocorrelation case (not considered here).

Table 5. Lagged Correlations of Salinity (Low-Pass Filtered) Between the Three Mooring Arrays^a

	Correlation Coefficient r						
	Salinity						
	DS 5	DS 6	DS 7	F2New	UK 1	G 1	UK 2
DS 1	0.08(2d)	0.19(1d)	-0.02(2d)	-0.15(11d)	-0.26(10d)	0.04(13d)	-0.18(16d)
DS 2	n.a.	n.a.	n.a.	0.24(8d)	0.26(13d)	-0.26(15d)	0.30(16d)
DS 5	-	-	-	0.57(8d)	0.64(11d)	0.73(12d)	0.74(14d)
DS 6	-	-	-	0.78(10d)	0.83(10d)	0.89(11d)	0.91(14d)
DS 7	-	-	-	0.73(10d)	0.79(10d)	0.82(11d)	0.85(14d)

^a(xxd): days of lag. n.a.: not available. Nonbolded numbers denote correlations below the 99% significance limit. Bolded numbers correspond to significant correlations. Dashes are filled in for the autocorrelation case (not considered here).

are present between the Denmark Strait sill array and the deep downstream. There is no overlapping period of measurements for DS 2 and DS 5/DS 6/DS 7, but correlations at Angmagssalik are even better than for DS 1. Up to 60% of the downstream temperature variance originates from anomalies seen at the sill of Denmark Strait.

The lagged correlations additionally indicate the propagation time scale of DSOW temperature anomalies along the slope of the Greenland shelf: anomalies originally recorded at the sill of Denmark Strait will be seen 2 days later at the entrainment array and further 10–14 days later at the Angmagssalik array. These propagation times thus correspond to mean current speeds in the order of 100 and 35 cm s⁻¹, respectively. The direct correlation from the Denmark Strait sill to Angmagssalik gives similar time scales of 8–16 days and mean current speeds of O(45 cm s⁻¹). These speeds probably underestimate the real mean flow, as lagged correlations reflect the combined effect of all advective-diffusive transports and not only the advection [Jeffress and Haine, 2014]. Within the uncertainty of the time lags (which is about 2 days), these results are in reasonable agreement and also conform with other studies (e.g., Eulerian estimates from moorings as in von Appen et al. [2014a] or Lagrangian estimates from a model in Koszalka et al. [2013]).

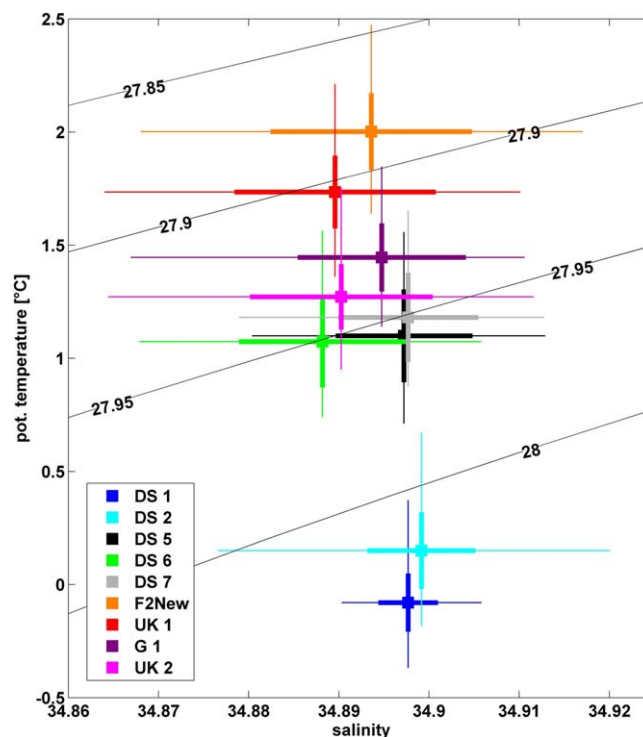


Figure 6. Potential temperature and salinity diagram for all low-pass filtered mooring records shown in Figures 4 and 5. The squares depict the average values, the thick horizontal and vertical lines the standard deviation of the mean, and the thin lines the maximum range of properties.

The disagreement with the average velocities of Table 1 can be explained by the missing velocity measurements in the region of the first 125 km downstream of the sill, where the plume accelerates and the highest mean velocity of approximately 70 cm s⁻¹ is found [Girton and Sanford, 2003].

The results from lagged correlations of the salinity time series differ dramatically from the temperature time series presented above. No significant correlation was found between the Denmark Strait sill array and any of the downstream salinity records (Table 5). This different behavior of the salinity variance at the Denmark Strait sill moorings is even apparent from a visual inspection of Figure 5. However, the propagation of salinity anomalies is clearly seen between the entrainment array and Angmagssalik, where the best agreement is evident between DS 6 and UK 2 ($r = 0.91$). In contrast to the temperature records, the

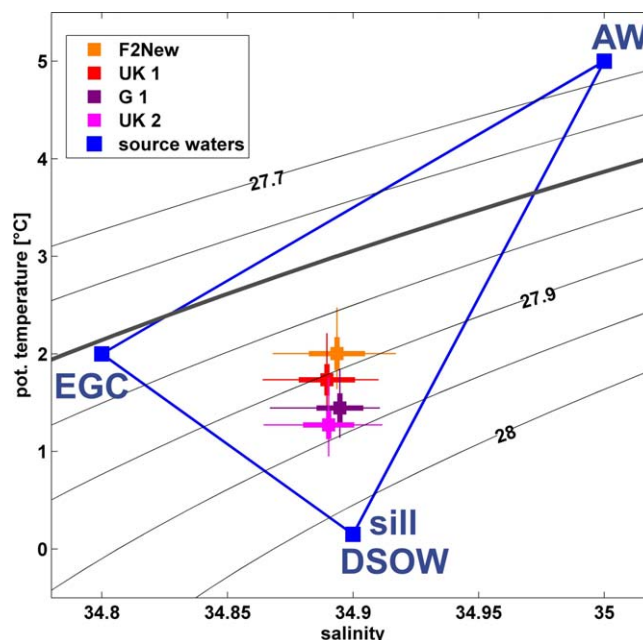


Figure 7. Potential temperature and salinity diagram for the Angmagssalik moorings (as in Figure 6) and the source waters used for the water mass analysis (see text for details). EGC: Water from the East Greenland Current; AW: Atlantic Water; sill DSOW: Denmark Strait overflow water as measured directly at the sill.

correlations of salinity anomalies are even significant for mooring F2New. Between 50% and 80% of the salinity variance at Angmagssalik can be explained by the anomalies found at the entrainment array. Salinity anomalies are thus mixed into the DSOW plume in the region between the Denmark Strait sill array and the entrainment array.

3.3. Water Mass Modification by Entrainment of Ambient Water

The change of hydrographic properties in DSOW descending into the North Atlantic is depicted in the potential temperature/salinity diagram in Figure 6. While the DSOW at the sill of Denmark Strait is limited to the salinity range 34.89–34.905 and between +0.5°C and –0.5°C, the downstream measurements allocate a much wider salinity space (34.865–34.905) and higher temperatures. The records

from the entrainment array are much closer to records obtained at Angmagssalik than to the Denmark Strait sill measurements. The DSOW modification is strongest between the Denmark Strait sill array and the entrainment array, where much of the salinity variance is induced by the entrainment of fresher water. Further downstream, only gradual warming occurs, especially at the deeper moorings at Angmagssalik.

A source of fresher water and enhanced salinity variability could be the low-salinity lid of the DSOW plume that is added downstream of the sill to the overflow layer and gradually mixed into the plume along its pathway [Rudels et al., 1999]. The lid water originates from the East Greenland Current Water, which combines several sources of low salinity (e.g., Polar Water and sea ice) and is the only source of fresher water in the area. In addition, the EGC also transports a dense water layer (Figure 1) [Våge et al., 2011; von Appen et al., 2014b]. As seen in the section of temperature and salinity at the sill, the shelf waters are indeed within the DSOW density range, but are warmer and fresher (between km –240 and –80 in Figure 1) than the waters in the deep channel (around km 0 in the figure). Within the first 180 km downstream from the sill, the shelf waters descend from the shelf and join the DSOW plume from the deep channel [Rudels et al., 2002]. The shelf waters are therefore an important source of the water masses available for entrainment. The East Greenland Spill Jet described for shelf sections obtained further south [Pickart et al., 2005] is characterized as an intermittent and local phenomenon, but is able to introduce considerable low-salinity anomalies into the DWBC [Brearley et al., 2012; Falina et al., 2012]. The shelf waters can either descend from the shelf due to topographic gaps in the continental shelf, or as spilling events [Koszalka et al., 2013]. Which of the two mechanisms is more important is unknown so far.

Table 6. Average Source Water Content With Standard Deviation for the Three Source Water Masses at the Angmagssalik Moorings^a

	Average Content ± Standard Deviation in %		
	Original DSOW	Atlantic Water	EGC Water
F2New	37 ± 4	30 ± 5	32 ± 7
UK 1	41 ± 6	24 ± 5	35 ± 7
G 1	52 ± 5	21 ± 3	27 ± 6
UK 2	55 ± 5	17 ± 4	28 ± 7

^aSee text for details.

Warm and saline Atlantic Water (AW) from the Irminger Current is the source for warming of the DSOW layer. AW can be identified as a neighboring water mass of DSOW from CTD profiles measured south of the Denmark Strait sill. A collection of nearly 500 CTD profiles [Nielsen et al., 2007] was used to obtain average properties of the

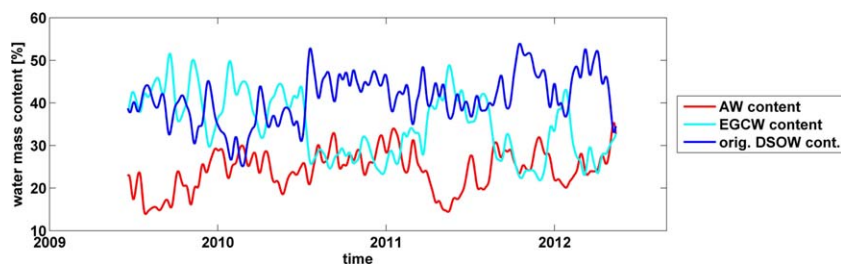


Figure 8. Water mass content for the Angmagssalik mooring UK 1. The DSOW at this location can be obtained by varying contributions of Atlantic Water (AW), East Greenland Current Water (EGCW), and original DSOW.

density layer $\sigma_\theta = 27.6\text{--}27.75 \text{ kg m}^{-3}$ south of Denmark Strait. The dominant temperature and salinity of the layer above the DSOW was then derived from histograms of these data (Figure S2 in the supporting information): the warm layer covering the overflow has a mean potential temperature of 5°C and 35 in salinity.

The DSOW found at Angmagssalik can be explained by the mixing of original DSOW from the Denmark Strait sill with EGC water and AW. The necessary fractions of each constituent can be estimated by the “mixing triangle” [e.g., Mamayev, 1975; Tomczak, 1981] as a linear combination of each of the three source water masses. As source water masses we use the respective endpoints in the temperature/salinity space, where the three components are located. These are: (1) the average properties of DS 2 (0.15°C and 34.9), which are used because of the better results in the correlations with the downstream data; (2) the EGC water as derived from the Falina *et al.* [2012] and Rudels *et al.* [2002] hydrographic measurements (2°C and 34.8); (3) the AW as the average properties of the neighboring water (cf. Figure S2) obtained from CTD measurements (5.0°C and 35.0). The analysis then calculates the relative contributions of these sources required to produce water with properties set to be those measured at the Angmagssalik moorings (cf. Figure 7).

The results from water mass analysis give estimated volume fractions for each of the three source waters for the records from Angmagssalik. The average volume fraction of original DSOW increases at the near-bottom instruments with increasing depth (Table 6), while the standard deviation of the volume fraction has a similar magnitude for all depths and source waters. Original DSOW from the sill provides the largest volume fraction at all moorings. At the shallow F2New, the contributions are nearly equally distributed. Entrainment of EGC waters has a larger contribution than AW at all moorings.

The seasonal cycle in the entrained contributions of the source waters is between 2% and 5%. Maximum contributions of AW (EGC water) occur in winter (summer); the AW and EGC water contributions are thus in antiphase and significantly correlated ($r = 0.6$). No seasonality is found in the original DSOW content, which is in agreement with the lack of a seasonal cycle in DSOW transports at the sill of Denmark Strait [Jochumsen *et al.*, 2012]. The seasonal behavior of the source water mass content is similar at all Angmagssalik moorings. An example of the temporal evolution of the three source water contributions is shown in Figure 8. The EGC water content is anticorrelated with the original DSOW content ($r = -0.74$) and with the AW content ($r = -0.60$). The content of original DSOW at the UK 1 mooring at Angmagssalik is additionally positively correlated with the transport of DSOW in Denmark Strait (volume transport time series from Jochumsen *et al.* [2012]) when a time lag of 16 days is applied.

4. Summary and Discussion

Low-pass filtered time series of near-bottom hydrographic and current measurements in the DSOW plume from moored instrumentation are compared for three different locations in the period 2007–2012. The average values of potential temperature reflect a rapid warming of about 1°C between the sill of Denmark Strait and the entrainment mooring array 180 km downstream (Table 1). During the second part of the plume’s descent (from the entrainment array to Angmagssalik, 370 km distance), the warming is between 0.8°C and 0.2°C , depending on the position of the measurement on the Greenland slope, with stronger warming at shallower bottom depths.

The more vigorous change of DSOW properties within the first 180 km from the sill is in agreement with previous studies [e.g., Voet and Quadfasel, 2010]. While the average salinity is similar at all locations (maximum 5 difference is 0.011), the salinity variance does increase downstream (Figure 6). The velocity is highest and most variable at the sill of Denmark Strait. The current strength is reduced at Angmagssalik, as well as its variance. Temperature and salinity anomalies are found to be coherent between the moorings in each array (Tables 2 and 3).

Lagged correlations indicate the advection of temperature anomalies from the sill of Denmark Strait to the entrainment and Angmagssalik arrays (Table 4) within 2 and 13 days, respectively. From these propagation times, an average propagation speed of 45 cm s^{-1} is obtained, which is in agreement with previous estimates [e.g., Quadfasel and Käse, 2007; Koszalka et al., 2013]. In contrast, salinity anomalies (as well as velocity anomalies) could not be traced from the Denmark Strait sill array to the downstream mooring locations. Only between the entrainment array and Angmagssalik are significant lagged correlations found (Table 5). The fresh anomalies present in the Angmagssalik time series are thus apparently not advected there as part of the dense bottom plume from Denmark Strait, but are injected within the first 180 km downstream of the sill by the entrainment of fresher water.

The most likely candidates for the entrainment into the descending DSOW plume are Atlantic Water and East Greenland Current Water. The EGC water consists of several sources, which are of Arctic as well as of Nordic Seas origin [e.g., Rudels et al., 2002; Sutherland and Pickart, 2008]. The entrained water is then not only Irminger Sea water but also from northern sources carried in the EGC that are mixed into the dense plume south of the sill. The amount of EGC water mixed into DSOW is thus responsible for the strength of fresh anomalies at Angmagssalik, whereas variations in salinity of the source waters in the Nordic Seas or in the Arctic as seen at the time series from Denmark Strait result only in salinity anomalies of half the amplitude.

This result is partly consistent with the hypothesis put forward by Holfort and Albrecht [2007] who attributed large freshening events in the DSOW plume to changes in the various contributions of different water masses to the formation of DSOW rather than changes in their properties, although their study connected to atmospheric forcing at the Denmark Strait sill. Hall et al. [2011] also connected fresh events at Angmagssalik with upstream atmospheric forcing arguing that they are caused by northerly wind anomalies north of Denmark Strait generating higher volume flux of EGC water to the sill rather than by changes in the properties of this source water. This is directly compatible with our finding that it is the amount of EGC water rather than its property anomalies that drives salinity variability in the DSOW plume. However, the results of our analysis disagree with their rejection of entrainment as an important source for fresh anomalies, which the authors themselves acknowledged was arguable. This conclusion of Hall et al. [2011] was based on a global model in which entrainment processes are underestimated (although they are eddy-resolving) and downstream overflow water is often represented at wrong depth levels [e.g., Xu et al., 2010]. Additionally, our work places the processes responsible for the anomalies to locations south of the Denmark Strait sill.

A water mass analysis has been performed, using EGC water and AW for entrainment, as well as the original DSOW from the sill. The results showed a depth-dependent contribution of the source waters at Angmagssalik (Table 6). The DSOW found at the shallow F2New mooring is composed nearly equally of the three sources. The original DSOW content increases with mooring depth (from F2New to UK 2) while the AW and EGC water contributions decrease. The AW content decreases greater than that of the EGC water content. The AW becomes the neighboring water mass of the DSOW plume from approximately 30 km downstream of the sill at 400–1000 m depth and is thus available for turbulent vertical mixing and lateral entrainment. EGC water is located on the East Greenland shelf and is thus not directly in contact with the DSOW in the deep channel. From our analysis, we confirm the possibility of the spilling events of dense shelf water, forming the East Greenland Spill Jet, to modify the DSOW layer within the DWBC substantially and persistently (as hypothesized before in Falina et al. [2012] and Magaldi et al. [2011]). The spilling relevant for DSOW occurs north of 65.3°N (the latitude of the entrainment array), as salinity anomalies can be traced from there to Angmagssalik. Spilling events further downstream might then only contribute to shallower layers, e.g., to Iceland Scotland overflow water. The water mass analysis does not agree with the possibility of increased spilling in winter (due to storms) [Magaldi et al., 2011], as maximum EGC water contents are found in summer (cf. Figure 8). Increased EGC contributions in summer rather support a hypothesis presented in Rudels et al. [1999, 2002] namely that the EGC

waters are divided into two layers by intrusions of recirculating Atlantic Water; the denser layer is a potential overflow contribution, and the other forms surface water. The level of separation is determined by the density of the AW in the Irminger Current. In summer, the AW is less dense and separates the EGC at a shallower density level allowing more low-salinity water to contribute to the overflow. In winter, the process is reversed. The EGC water mass characteristics are (except at the surface) set farther north and are not affected by the seasonality.

Nevertheless, other ambient water masses may additionally contribute to the mixing into the DSOW plume; the choice of only three sources, caused by the limited amount of measured properties, may be too simplistic. Additional candidates for mixing in the Irminger Sea are Labrador Sea Water (LSW), Northeast Atlantic Deep Water (NEADW), or Lower Deep Water (LDW), which is modified Antarctic Bottom Water. LSW found in the central Irminger Sea (J. Karstensen, personal communication, 2012) is 2°C–3°C warmer than the DSOW, but in the same salinity range, and was not found in close vicinity to the Denmark Strait sill. NEADW, formed of modified ISOW, is more saline than DSOW and also warmer [Dickson and Brown, 1994]. LDW is not found in the relatively shallow area where the DSOW descends into the Irminger Basin. Therefore, the choice of the three sources of original DSOW, EGC water, and AW can be considered realistic for the entrainment regime just downstream of Denmark Strait.

The results from the water mass analysis for the Angmagssalik hydrographic data using three sources obviously depends strongly on the choice of source waters. The relevant EGC water may be somewhat colder and fresher than the gauged values used here. Additionally, the AW properties obtained from the CTD data were extracted from density levels close to the DSOW, although warmer and saltier surface waters could be the original source. Simultaneous changes of $\pm 0.5^\circ\text{C}$ in temperature and ± 0.05 in salinity in the definition of the source waters cause deviations of up to 20% in volume fraction of each water mass contribution. Applying more extreme source properties for EGC water and AW enlarges the mixing triangle in T/S space (Figure 7) and changes the relative contributions of the sources, but not the variability depicted in Figure 8. Finally, variability present in the source water masses was neglected due to the lack of time series from the EGC waters and AW.

Despite these uncertainties, the amount of EGC water present at the Angmagssalik moorings derived from this study is remarkably close to other estimates. Koszalka *et al.* [2013] obtained from their Lagrangian model study a contribution of 26% EGC particles at Angmagssalik (their SHELF and KANGER contributions); Falina *et al.* [2012] used synoptic ship sections and attributed 25% of the DWBC transport near Cape Farewell to cascading shelf waters. Our estimate of about 30% EGC water at Angmagssalik fits well within these numbers (Table 6). Overall, about 75% of the water forming the DSOW layer at Angmagssalik originates from north of Denmark Strait and is transferred to deep waters in the North Atlantic.

The final conclusion of our study is that DSOW anomalies found in the DWBC far away from Denmark Strait cannot be directly interpreted as Arctic variability. This holds especially for salinity anomalies, which were found to be a consequence of mixing processes. DSOW anomalies can originate from variability of the DSOW sources in the Nordic Seas, changes in the rate of entrainment, or variations in the entrained water mass properties. All three of these processes together contribute to the variability found at Angmagssalik. In our work, we attributed salinity anomalies to be a result from changes in the entrainment, while variability in the Nordic Seas was not contributing substantially (as seen in the lagged correlations). Therefore, the probability of identifying fresh anomalies originating in the Arctic on an advective path from the sill of Denmark Strait southward is low. Following temperature anomalies downstream is more promising, although the explained variance in temperature at Angmagssalik is below 50% on average using the Denmark Strait sill moorings. With increasing distance from Denmark Strait this value decreases and even the tracking of temperature anomalies becomes challenging.

Although the Nordic Seas overflows were found to control the DWBC along the Greenland slope and thus the Atlantic Meridional Overturning Circulation (AMOC) in the Irminger Basin in models [Redler and Böning, 1997], our results suggest that entrainment hides Arctic climate anomalies and adds additional variability of larger amplitude. Establishing the link between Arctic variability and the deep limb of the AMOC through observations is therefore difficult. In order to fully understand the circulation and mixing at the East

Greenland slope, not only time series measured directly at the sill of Denmark Strait and of the overflow plume postentrainment are needed, but also of the entrained water masses: on the East Greenland Shelf and in the Atlantic Water layer and of the entrainment process itself.

Acknowledgments

We thank the many ship crews, chief scientists, and mooring technicians without whom the data would not have been collected. Shipboard and mooring data are available upon request from the authors or via the NAACLIM project website (<http://naclim.zmaw.de/>). Rolf H. Käse and Hendrik van Aken are acknowledged for helpful discussions. The research leading to these results has received funding from the European Union 7th Framework Program (FP7 2007–2013) under grant agreement 308299 (NAACLIM project) and grant GA212643 (THOR project). Additional support was given by the Cooperative project “RACE—Regional Atlantic Circulation and Global Change” funded by the German Federal Ministry for Education and Research (BMBF), 03f0651a. Cefas moorings were designed and deployed by John Read and Neil Needham; the work was also funded by the UK Department for Environment, Food and Rural Affairs (DEFRA) projects, SD0440, ACME-ME5102, and ForeDec ME5317. Hydrographic data of the Atlantic water layer in the northern Irminger Basin were provided by: Marine Research Institute, Iceland; Institute of Marine Research, Norway; Faroese Fisheries Laboratory; Arctic and Antarctic Research Institute, Russia, and Geophysical Institute, University of Bergen, Norway, through the NISE project. Finally we acknowledge two anonymous reviewers for their help in improving the manuscript.

References

- Brearley, J., R. Pickart, H. Valdimarsson, S. Jonsson, R. Schmitt, and T. Haine (2012), The East Greenland boundary current system south of Denmark Strait, *Deep Sea Res., Part I*, 63, 1–19.
- Dickson, B., J. Meincke, I. Vassie, J. Jungclauss, and S. Østerhus (1999), Possible predictability in overflow from the Denmark Strait, *Nature*, 397, 243–246.
- Dickson, B., I. Yashayaev, J. Meincke, B. Turrell, S. Dye, and J. Holfort (2002), Rapid freshening of the deep North Atlantic Ocean over the past four decades, *Nature*, 416, 832–837.
- Dickson, B., et al. (2008), The overflow flux west of Iceland: Variability, origins and forcing, in *Arctic-Subarctic Ocean Fluxes: Defining the Role of the Northern Seas in Climate*, edited by R. R. Dickson, J. Meincke, and P. Rhines, pp. 443–474, Springer, Netherlands, doi:10.1007/978-1-4020-6774-7_20.
- Dickson, R., and J. Brown (1994), The production of North Atlantic Deep Water: Sources, rates, and pathways, *J. Geophys. Res.*, 99(C6), 12,319–12,341.
- Falina, A., A. Sarafanov, H. Mercier, P. Lherminier, A. Sokov, and N. Danialt (2012), On the cascading of dense shelf waters in the Irminger Sea, *J. Phys. Oceanogr.*, 42, 2254–2267, doi:10.1175/JPO-D-12-012.1.
- Fischer, J., et al. (2014), Intra-seasonal variability of the Deep Western Boundary Current in the western subpolar North Atlantic, *Prog. Oceanogr.*, doi:10.1016/j.pocean.2014.04.002, in press.
- Girton, J., and T. Sanford (2003), Descent and modification of the overflow plume in the Denmark Strait, *J. Phys. Oceanogr.*, 33, 1351–1364.
- Girton, J., T. Sanford, and R. Käse (2001), Synoptic sections of the Denmark Strait overflow, *Geophys. Res. Lett.*, 28(8), 1619–1622.
- Hall, S., S. Dye, K. Heywood, and M. Wadley (2011), Wind forcing of salinity anomalies in the Denmark Strait overflow, *Ocean Sci.*, 7, 821–834, doi:10.5194/os-7-821-2011.
- Hansen, B., S. Østerhus, D. Quadfasel, and W. Turrell (2004), Already the day after tomorrow?, *Science*, 305, 953–954, doi:10.1126/science.1100085.
- Holfort, J., and T. Albrecht (2007), Atmospheric forcing of DSOW salinity, *Ocean Sci.*, 3, 411–416.
- Jeffress, S., and T. Haine (2014), Correlated signals and causal transport in ocean circulation, *Q. J. R. Meteorol. Soc.*, 140, 2375–2382, doi:10.1002/qj.2313.
- Jochumsen, K., D. Quadfasel, H. Valdimarsson, and S. Jónsson (2012), Variability of the Denmark Strait overflow: Moored time series from 1996–2011, *J. Geophys. Res.*, 117, C12003, doi:10.1029/2012JC008244.
- Käse, R., J. Girton, and T. Sanford (2003), Structure and variability of the Denmark Strait overflow: Model and observations, *J. Geophys. Res.*, 108(C6), 3181, doi:10.1029/2002JC001548.
- Koszalka, I., T. Haine, and M. Magaldi (2013), Fates and travel times of Denmark Strait overflow water in the Irminger Basin, *J. Phys. Oceanogr.*, 43, 2611–2628, doi:10.1175/JPO-D-13-023.1.
- Macrander, A., U. Send, H. Valdimarsson, S. Jónsson, and R. H. Käse (2005), Interannual changes in the overflow from the Nordic Seas into the Atlantic Ocean through Denmark Strait, *Geophys. Res. Lett.*, 32, L06606, doi:10.1029/2004GL021463.
- Macrander, A., R. H. Käse, U. Send, H. Valdimarsson, and S. Jónsson (2007), Spatial and temporal structure of the Denmark Strait Overflow revealed by acoustic observations, *Ocean Dyn.*, 57, 75–89, doi:10.1007/s10236-007-0101-x.
- Magaldi, M., T. Haine, and R. Pickart (2011), On the nature and variability of the East Greenland Spill Jet: A case study in summer 2003, *J. Phys. Oceanogr.*, 41, 2307–2327, doi:10.1175/JPO-D-10-05004.1.
- Mamayev, O. (1975), *Temperature-Salinity Analysis of World Ocean Waters*, 374 pp., Elsevier, Amsterdam.
- Nielsen, J., H. Hatun, K. Mork, and H. Valdimarsson (2007), The NISE dataset, technical report 07-01, Faroese Fish. Lab., Tórshavn.
- Paka, V., B. Rudels, D. Quadfasel, and V. Zhurbas (2010), Measurements of turbulence in the zone of strong bottom currents in the Strait of Denmark, *Dokl. Earth Sci.*, 432, 613–617.
- Paka, V., V. Zhurbas, B. Rudels, D. Quadfasel, A. Korzh, and D. Delisi (2013), Microstructure measurements and estimates of entrainment in the Denmark Strait overflow plume, *Ocean Sci. Discuss.*, 10, 1067–1098, doi:10.5194/osd-10-1067-2013.
- Pickart, R., D. Torres, and P. Fratantoni (2005), The East Greenland Spill Jet, *J. Phys. Oceanogr.*, 35, 1037–1053.
- Quadfasel, D., and R. Käse (2007), Present-day manifestation of the Nordic Seas Overflows, in *Ocean Circulation: Mechanisms and Impacts*, *Geophys. Monogr. Ser.*, vol. 173, edited by A. Schmittner et al., pp. 75–90, AGU, Washington, D. C., doi:10.1029/173GM07.
- Redler, R., and C. Böning (1997), Effect of the overflows on the circulation in the subpolar North Atlantic: A regional model study, *J. Geophys. Res.*, 102(C8), 18,529–18,552.
- Rudels, B., P. Eriksson, H. Grönvall, R. Hietala, and J. Launiainen (1999), Observations in Denmark Strait in Fall 1997, and their implications for the entrainment into the overflow plume, *Geophys. Res. Lett.*, 26(9), 1325–1328.
- Rudels, B., E. Fahrbach, J. Meincke, G. Budéus, and P. Eriksson (2002), The East Greenland Current and its contribution to the Denmark Strait overflow, *ICES J. Mar. Sci.*, 59, 1133–1154, doi:10.1006/jmsc.2002.1284.
- Spall, M., and J. Price (1998), Mesoscale variability in Denmark Strait: The PV outflow hypothesis, *J. Phys. Oceanogr.*, 28, 1598–1623.
- Sutherland, D., and R. Pickart (2008), The East Greenland Coastal Current: Structure, variability, and forcing, *Prog. Oceanogr.*, 78, 58–77, doi:10.1016/j.pocean.2007.09.006.
- Swaters, G. (1991), On the baroclinic instability of cold-core coupled density fronts on a sloping continental shelf, *J. Fluid Mech.*, 224, 361–382.
- Tanhua, T., K. Olsson, and E. Jeansson (2005), Formation of Denmark Strait overflow water and its hydro-chemical composition, *J. Mar. Syst.*, 57, 264–288.
- Tomczak, M. (1981), A multi-parameter extension of temperature/salinity diagram techniques for the analysis of non-isopycnal mixing, *Prog. Oceanogr.*, 70, 147–171.
- Våge, K., R. Pickart, M. Spall, H. Valdimarsson, S. Jónsson, D. Torres, S. Østerhus, and T. Eldevik (2011), Significant role of the North Icelandic Jet in the formation of Denmark Strait overflow water, *Nat. Geosci.*, 4, 723–727, doi:10.1038/NCEO1234.

- van Aken, H., and M. de Jong (2012), Hydrographic variability of Denmark Strait overflow water near Cape Farewell with multi-decadal to weekly time scales, *Deep Sea Res., Part I*, *66*, 41–50.
- Voet, G., and D. Quadfasel (2010), Entrainment in the Denmark Strait overflow plume by meso-scale eddies, *Ocean Sci.*, *6*, 301–310.
- von Appen, W., R. Pickart, K. Brink, and T. Haine (2014a), Water column structure and statistics of Denmark Strait overflow water cyclones, *Deep Sea Res., Part I*, *84*, 110–126, doi:10.1016/j.dsr.2013.10.007.
- von Appen, W., et al. (2014b), The East Greenland Spill Jet as an important component of the Atlantic meridional overturning circulation, *Deep Sea Res., Part I*, *92*, 75–84, doi:10.1016/j.dsr.2014.06.002.
- Whitehead, J. (1998), Topographic control of oceanic flows in deep passages and straits, *Rev. Geophys.*, *36*(3), 423–440.
- Xu, X., W. Schmitz, H. Hurlburt, P. Hogan, and E. Chassignet (2010), Transport of Nordic Seas overflow water into and within the Irminger Sea: An eddy-resolving simulation and observations, *J. Geophys. Res.*, *115*, C12048, doi:10.1029/2010JC006351.